Carbohydrate Polymers 229 (2020) 115487

Contents lists available at ScienceDirect

Carbohydrate Polymers

journal homepage: www.elsevier.com/locate/carbpol

Structural characterization and antiviral activity of two fucoidans from the brown algae *Sargassum henslowianum*

Qi-Li Sun[a,c,1], Yi Li[b,1], Long-Quan Ni[b], Yi-Xuan Li[a,c], Yong-Sheng Cui[a], Si-Liang Jiang[a,c], En-Yi Xie[d], Juan Du[c], Fei Deng[b,*], Cai-Xia Dong[a,*]

[a] Tianjin Key Laboratory on Technologies Enabling Development of Clinical Therapeutics and Diagnosis, School of Pharmacy, Tianjin Medical University, Tianjin 300070, China
[b] State Kay Laboratory of Virology and National Virus Resource Center, Wuhan Institute of Virology, Chinese Academy of Sciences, Wuhan 430071, China
[c] Department of Pharmacognosy, College of Pharmacy, Jiamusi University, Jiamusi 154007, China
[d] College of Fisheries, Guangdong Ocean University, Zhanjiang 524088, China

ARTICLE INFO

Keywords:
Brown algae
Sargassum henslowianum
Fucoidans
Antiviral
Herpes simplex virus

ABSTRACT

Purified fucoidans SHAP-1 and SHAP-2 with apparent molecular weights of 6.55×10^5 and 5.89×10^5, respectively, were isolated from *Sargassum henslowianum* by ion-exchange and gel-filtration column chromatography. They are both composed of fucose and galactose at a ratio of around 3:1 and 31.9% sulfate. The backbone of two fucoidans consists of α-(1→3)-linked L-Fuc*p* residues which are mainly sulfated on the C-2 and C-4 positions. Side chains composed of terminally linked α-L-Fuc*p* and α-D-Gal*p* residues, and (1→2)-, (1→6)-, and (1→2,6)-linked β-D-Gal*p* residues attach mainly at *O*-4 position of backbone residues. Antiviral test showed that the IC_{50} values of SHAP-1 and SHAP-2 against HSV-1 were estimated to be 0.89 and 0.82 μg/mL by plaque reduction assay, respectively, whereas both as low as 0.48 μg/mL against HSV-2. The antiviral mechanism of the fucoidans might be at least through blocking HSV-2 virion adsorption to host cells. These results suggest that the fucoidans have potential clinical applications.

1. Introduction

Herpes simplex viruses (HSVs) are common pathogens that seriously harm human health. Herpes simplex virus type 1 (HSV-1) frequently causes ocular or oral-facial infections. HSV-1 infection can also cause encephalitis, which may be fatal. Herpes simplex virus type 2 (HSV-2) is mostly responsible for genital herpes (Shukla & Spear, 2001), which is a highly prevalent sexually transmitted disease worldwide (Groves, 2016; Looker et al., 2017). Epidemiological findings showed that HSV-2 is transmitted by direct body contact with infected lesions or body fluids, infects the mucosal tissues or lesions of the skin, and causes the characteristic lifelong latent infection. In addition, primary HSV-2 infection transmitted to the newborn is associated with high morbidity and mortality (Awasthi et al., 2015). Importantly, HSV-2 increases human immunodeficiency virus (HIV) acquisition and transmission (Finger-Jardim et al., 2014; Freeman et al., 2006; Looker et al., 2015). When the immune system is impaired, HSV-2 invades immune surveillance and causes recurrent symptoms (Roizman, Knipe, & Whitley, 2007). In recent years, acyclovir (ACV), a representative of nucleoside analogs, has been clinically used for treating HSV infection in immunocompetent patients (Jaishankar & Shukla, 2016). However, similar to other anti-herpetic agents for treating HSV-2 infection, acyclovir cannot eradicate the virus from infected cells and prevent the recurrence of HSV because it cannot counteract early HSV infection (Gnann, Barton, & Whitley, 1983). In addition, recent studies have observed drug resistance, especially in immunocompromised persons, implicating an increasing risk of HSV recurrence (Chatis & Crumpacker, 1991; Posavad, Koelle, Shaughnessy, & Corey, 1997; Swetter et al., 1998). In this regard, new drugs with novel mode of action are in high demand.

Natural products represent a rich platform for the development of new biologically active compounds and drug candidates. In this way, many investigators have attempted to search for new, effective antiviral drugs from natural sources. Marine brown algae of the class Phaeophyceae are a rich source of unique polysaccharides. Abundantly found in marine brown algae, fucoidan is a fucose-containing sulfated polysaccharide with complex, heterogeneous structures that contain fucose, sulfate groups, and other components, such as galactose, xylose,

* Corresponding authors.
E-mail addresses: df@wh.iov.cn (F. Deng), dongcaixia@tmu.edu.cn (C.-X. Dong).
[1] These authors contributed equally to the manuscript.

https://doi.org/10.1016/j.carbpol.2019.115487
Received 12 August 2019; Received in revised form 25 September 2019; Accepted 15 October 2019
Available online 20 October 2019
0144-8617/

mannose, and uronic acids (Kwak, 2014; Pomin & Mourao, 2008). Recent studies have shown that fucoidan in marine brown algae consistently exhibits beneficial effects, such as anticancer (Schneider, Ehrig, Liewert, & Alban, 2015; Cho et al., 2016; Han et al., 2017; Hsu et al., 2017; Rui, Pan, Shao, & Xu, 2017; Anastyuka et al., 2017; Usoltseva, Anastyuk, Shevchenko, Zvyagintseva, & Ermakova, 2016, 2018; Usoltseva et al., 2019), anti-oxidative (Wu, Wu, Qu, Li, & Yan, 2013), immunological (Cho, Lee, Kim, & You, 2014; Han, Sun, Li, Wu, & Nie, 2018; Zhang et al., 2016), anti-inflammatory (Islam et al., 2013; Sanjeewa et al., 2017), and anti-virus (Sinha, Astani, Ghosh, Schnitzler, & Ray, 2010; Thuy et al., 2015), which depend on their structural characteristics, such as molecular weight, sulfation pattern, and monosaccharide composition (Ale, Maruyama, Tamauchi, Mikkelsen, & Meyer, 2011; Ghosh et al., 2009; Sanjeewa et al., 2018).

Sargassum henslowianum is a brown alga widely distributed in southeastern China and southeast Asia. Several polysaccharides isolated from the genus *Sargassum* exhibit anti-HSV activity (Zhu, Ooi, Chan, & Ang, 2004; Zhu, Ooi, Chan, & Ang, 2003; Ghoshet al., 2009; Lee, Takeshita, Hayashi, & Hayashi, 2011; Sinha et al., 2010). These results suggest us the polysaccharides from *S. henslowianum* may also possess well anti-HSV activity. Few reports, however, have focused on the structure and antiviral activities of fucoidans, except to two fucoidans showed hypolipidemic and immunomodulatory activities (Cuong, Thuy, Huong, Ly, & Van, 2015; Han et al., 2018). In the present study, we investigated the chemical structures of two purified sulfated polysaccharides isolated from *S. henslowianum* and their in vitro anti-HSV activities and further demonstrated their antiviral mode of action.

2. Materials and methods

2.1. Materials and general methods

S. henslowianum was collected in April 2015 at Zhanjiang City, Guangdong Province, China. A voucher specimen has been deposited at the Laboratory of Pharmacognosy, School of Pharmacy, Tianjin Medical University, China. DEAE-650 M, and Sephacryl S-500 HR were purchased from GE Healthcare Life Sciences (Amersham Biosciences AB, Uppsala, Sweden). Monosaccharide standards T-series dextrans and 1-phenyl-3-methyl-5-pyrazolone (PMP) were obtained from Sigma (St. Louis, MO, USA). *m*-Hydroxydiphenyl was purchased from Beijing Dingguo Changsheng Biotech Co., Ltd. Other analytical reagents were purchased from Tianjin Benchmark Chemical Reagent Co., Ltd.

High-performance liquid chromatography analysis (HPLC) was conducted on an Agilent 1260 Infinity II system equipped with ELSD. Gas chromatography–mass spectrometry (GC–MS) was carried out on an Agilent GCMS-5975 instrument with helium as the carrier gas.

2.2. Extraction, isolation and purification of polysaccharides

The brown alga *S. henslowianum* (800 g) were pulverized and then defatted twice by 95% ethanol (EtOH), each time for 12 h, as shown in Fig. 1. The residue was further extracted thrice by using distilled hot water under reflux, 2 h for each time. After filtration through defatted cotton and concentration in vacuo, the water extract was centrifuged at 3000 rpm for 20 min to remove the insoluble portion. The supernatant was concentrated and precipitated with 80% EtOH (final concentration) for three times at 4 ℃ overnight. The precipitates were re-dissolved and dialyzed against distilled water (cut off, 12,000 Da). The non-dialysate was lyophilized to obtain a crude polysaccharide fraction of SHCP (40.5 g, 5.1%).

SHCP was suspended in H_2O again, stirred at room temperature overnight, and then centrifuged at 3000 rpm for 20 min to remove insoluble portions. The supernatant was loaded on a Toyopearl DEAE 650 M column (5.0 i.d. × 20 cm), which were successively eluted with H_2O; 0.5, 1.0, and 2.0 M NaCl; and 0.2 M NaOH solution. Fractions of 15 mL were collected and monitored at 490 nm by the phenol–sulfuric acid (H_2SO_4) method (Dubois, Gilles, Hamilton, Rebers, & Smith, 1956) and UV absorbance at 280 nm. As a result, two major fractions named SHN (24.6%) eluted with H_2O and SHA2 (24.8%) eluted with 1.0 M NaCl solution were obtained. The fraction SHA2 was re-chromatographed and eluted through a linear elution program under 0–1 M NaCl to yield four fractions (SHA2A, SHA2B, SHA2C, and SHA2D). SHA2C was the major fraction, accounting for 47.3% of the mother fraction SHA2. SHA2C was then separated by gel permeation chromatography on a Sepharose 6 B column (5.0 i.d. × 100 cm) (Supporting Fig. 1-S(A)) to yield two major fractions, SHA2C-1 and SHA2C-2, which were further purified by gel permeation chromatography on a Sepharcryl S-500 HR column (2.2 i.d. × 100 cm) (Supporting Fig. 1-S(B and C)) to yield purified polysaccharide SHAP-1 (688 mg) and SHAP-2 (445 mg), respectively. Fractions of 10 mL were collected and monitored at 490 nm via the phenol − H_2SO_4 method and at 280 nm via UV absorbance spectroscopy.

2.3. Homogeneity and apparent molecular weight determination of polysaccharides

The apparent molecular weights of SHAP-1 and SHAP-2 were estimated on the PL aquagel-OH MIXED-H column (7.5 mm × 300 mm, 8 μm) and eluted with 0.1 M $NaNO_3$ at 0.6 mL/min with column temperature maintained at 35 ℃. Commercially available T-series dextrans (MW 2000, 670, 410, 270, 150, 80, 50, 12, 5, and 1 kD) were used as standard molecular markers.

2.4. Physicochemical properties

The contents of total carbohydrate and uronic acid were determined by the phenol − H_2SO_4 method (Dubois et al., 1956) and *m*-hydroxydiphenyl method (GustavAsboe-Hansen, 1973), respectively. Galactose and galacturonic acid were used as standards. Protein content determination was conducted using a Bio-Rad protein assay kit with BSA as the standard.

Infrared spectra (IR) of polysaccharides were recorded with a Nicolet 5700 FTIR Spectrometer (Thermo Co. Ltd., USA) in the range of 4000–400 cm^{-1} using the KBr-disk method. Ester sulfate content was determined on Elementarvario EL cube (Elementar Analysen systeme GmbH, Germany) and calculated using the following equation (Lim et al., 2016): Ester sulfate (%) = S% × 3.22, where S% is the content of sulfur.

2.5. Sugar composition analysis

Sugar composition of the polysaccharides was analyzed by the modified pre-column PMP-derivatives of carbohydrates (Honda et al., 1989). In brief, the polysaccharide sample (1 mg) was hydrolyzed with 1 mL of 2 M trifluoroacetic acid (TFA) at 120 ℃ for 2 h. The hydrolysates were subjected to drying under N_2 stream to remove the residual TFA. The resulting products were re-dissolved with 600 μL of 0.6 M NaOH. Subsequently, an equal volume of 0.5 M PMP methanolic solution was added into the residue solution. The mixture was allowed to react at 70 ℃ for 30 min. After cooling down to the room temperature, 100 μL of 0.6 M HCl was added to neutralize the reaction solution. Then, an equal volume of chloroform was added to the neutralized solution. After vigorous shaking followed by centrifugation, the organic phase was carefully discarded to remove the excess PMP reagents. The extraction process was repeated six times, and the aqueous layer was filtered through a syringe filter (0.45 μm) before HPLC analysis. Using the same method, we prepared the PMP-derived monosaccharide standard containing seven types of monosaccharides (Rha, Ara, Fuc, Man, Glc, Gal, and Rib) and two types of uronic acids (GlcA and GalA). The resulting PMP-derivatized samples and mixed monosaccharide standard were analyzed by an HPLC-DAD system equipped with a ZORBAXDB-C_{18} column (4.6 × 250 mm, 5 μm, Agilent, USA). The

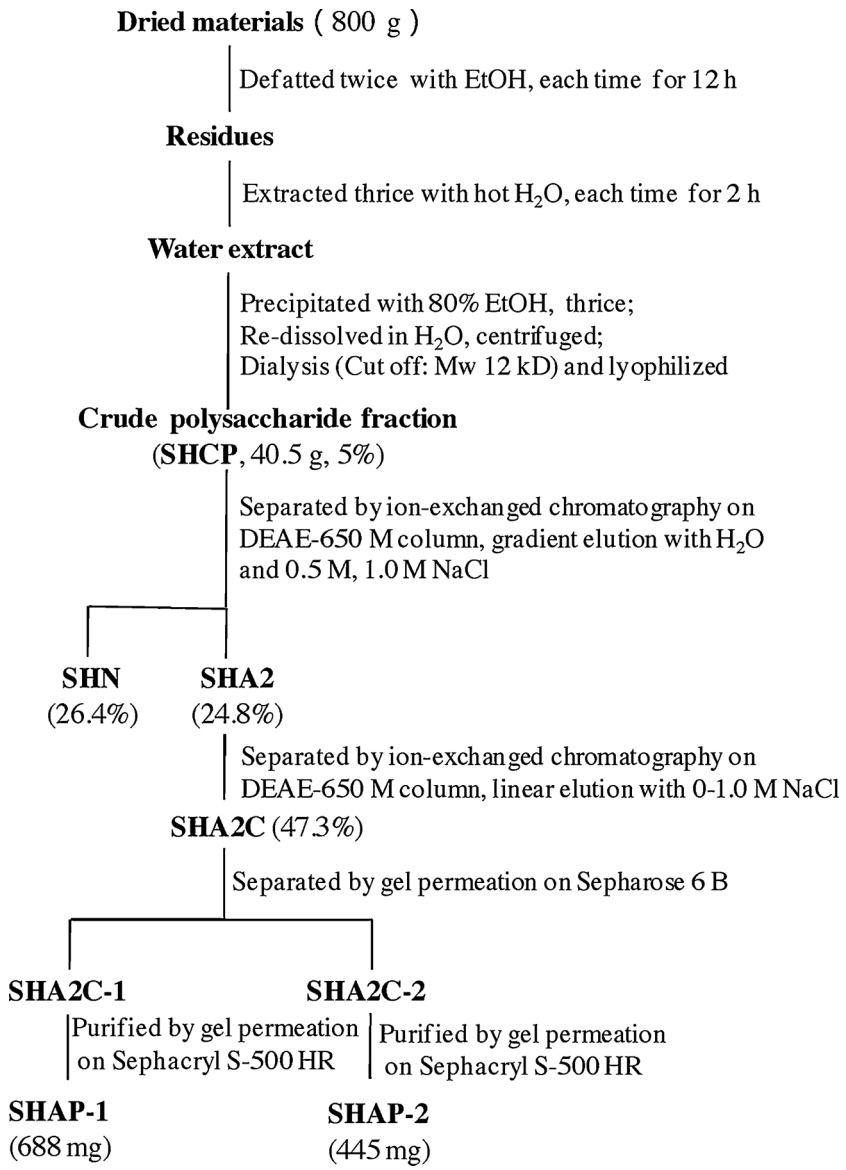

Fig. 1. The flow chart of purified polysaccharides (SHAP-1 and SHAP-2) from *Sargassum henslowianum*.

separation was achieved using gradient elution with 100 mM ammonium acetate aqueous solution (A) and acetonitrile (B) at a flow rate of 1.0 mL/min: 0–5 min, 17%–20% B; 5–35 min, 20%–27% B. Column temperature was set at 30 ℃. The UV detection wavelength was set at 245 nm.

2.6. Desulfation of polysaccharides

Desulfation of SHAP-1 and SHAP-2 was performed as previously described (Nagasawa, Inoue, & Tokuyasu, 1979). In brief, SHAP-1 and SHAP-2 (100 mg) were desalted through a Dowex 50 W × 8 resin (H^+ form, 2 × 20 cm) column eluted with H_2O. After neutralization with pyridine, the solution was lyophilized. The resulting pyridinium salt of polysaccharide was dissolved in 10% MeOH/dimethyl sulfoxide (10 mL) and then refluxed at 80 ℃ for 5 h with continuous stirring. After exhaustive dialysis against distilled H_2O, the reaction mixture was lyophilized to yield desulfated SHAP-1 and SHAP-2, named DS-SHAP-1 and DS-SHAP-2, respectively.

2.7. Methylation analysis

Equal amounts of native and desulfated SHAP-1 and SHAP-2 were methylated, respectively, as previously described by Ciucanu (Ciucanu & Kerek, 1984). The resulting products were hydrolyzed, reduced, and acetylated to form partially methylated alditol acetates (PMAA). The PMAA were subjected to GC–MS analysis using a HP-5MS fused silica capillary column (30 m × 0.25 mm i.d., 0.25 μm, Agilent, USA). The column temperature was set at 120 ℃ upon injection, increased at the rate of 4 ℃/min to 280 ℃, and then maintained at 280 ℃ for 5 min. Helium was used as the carrier gas. The compound that corresponded to each peak was identified through the interpretation of characteristic mass spectra and references. Peak area was used to calculate the molar ratio of each residue.

2.8. Nuclear magnetic resonance spectral analysis

SHAP-1 and SHAP-2 (60 mg) were dried in a vacuum over P_2O_5 for 72 h and then exchanged with deuterium by three cycles of lyophilization with D_2O (0.5 mL) before dissolution in D_2O. NMR spectra were obtained on a Varian INOVA 300 NMR spectrometer at room

temperature.

2.9. Cells and viruses

The African green monkey kidney (Vero) cell line (No.CCL-81) used in this study was purchased from ATCC. The cells were cultured in Dulbecco's modified Eagle medium (Thermo Fisher Scientific) supplemented with 10% fetal bovine serum (Gibco) at 37 ℃ with 5% CO_2. HSV-1 (F) and HSV-2 (333) were provided by the Microorganisms and Viruses Culture Collection Center, Wuhan Institute of Virology, CAS (serial number: IVCAS6.0182, IVCAS6.0183). Virus stocks were prepared on Vero cells, and the virus titer was determined by standard plaque assays.

2.10. Cytotoxicity assay

2.10.1. Cell countingkit-8 assay

Cell viability was assessed using the Cell Counting Kit-8 (Beyotime, PRC) in accordance with the manufacturer's instructions. In brief, the cells were seeded in a 96-well plate at a density of 5×10^3 cells/well in the absence or presence of various concentrations (0, 16, 80, 400, 1000, 2000 or 5000 μg/mL) of the polysaccharides in triplicate and then incubated at 37 ℃ in a humid atmosphere of 5% CO_2 for 72 h. The cells were washed once with phosphate-buffered saline (PBS, pH7.4), and then 100 μL fresh medium with 10 μL of WST-8 dye was added to each well. The plate was then incubated at 37 ℃ for 2 h. The absorbance was determined using a microplate reader at 450 nm (Synergy H1, Bio Tek).

2.10.2. Flow cytometry assay

Death cell ratio was measured by flow cytometry. Vero cells were seeded in a 12-well plate at a density of 5×10^4 cells/well, which was either in the absence or presence of various concentrations (0, 0.1, 1, 10, 100, or 1000 μg/mL) of the polysaccharides at 37 ℃ with 5% CO_2 for 72 h. The cells were digested with 2.5% trypsin and then washed twice with PBS. The cell suspension (100 μL) was stained with 5 μL of propidiumiodide (PI) for 30 min in the dark. PI-stained cells were analyzed by flow cytometry (BD Biosciences).

2.11. Antiviral activity assay

The antiviral activity assay was performed as previously described (Du et al., 2017) by a plaque reduction assay. Briefly, the confluent monolayers were infected with HSV-1 or HSV-2 (100 PFU/well) in the absence or presence of polysaccharides in serial concentrations (0, 0.1, 1, 10, 100, or 1000 μg/mL of SHAP-1 or SHAP-2 under HSV-1 infection and 0, 0.1, 0.125, 0.25, 0.5, 1, 10 or 100 μg/mL of SHAP-1 or SHAP-2 under HSV-2 infection). After the virus-polysaccharide mixtures were incubated for 1 h at 37 ℃ with gentle rocking, the cells were covered with overlay medium with 2% agarose and further incubated at 37 ℃ for 72 h. The plaques were fixed and visualized by staining with crystal violet. After air-dried, the number of plaques was counted. The degree of inhibition was expressed as inhibitory concentration (IC_{50}) which was calculated as the concentration of polysaccharides required to reduce plaque number up to 50% (IC_{50}). Antiviral activities were estimated by the selectivity index (SI) calculated from the CC_{50} and IC_{50} values.

2.12. Time-of-addition experiments

Vero cell monolayers were infected with HSV-2 (100 PFU/well) at 37 ℃ for 1 h. SHAP-1 and SHAP-2 were added at a concentration of 0.1 or 1.0 μg/mL before virus infection (preinfection treatment, 3 h before infection), during viral infection for 1 h (simultaneous treatment, i), or after virus infection (postinfection treatment, at 0 h post-infection (p.i.), 1 h p.i., 3 h p.i., and 6 h p.i.). At 10 h p.i., the incubation was removed further incubated at 37 ℃ until plaques formed. The degree of inhibition was calculated as follows:

$$\text{Inhibition (\%)} = \frac{\text{mean number of plaques in control} - \text{mean number of plaques in test}}{\text{mean number of plaquesin control}} \times 100 \quad (1)$$

2.13. Virus adsorption and penetration assays

The inhibitory effect of polysaccharides on HSV-2 adsorption to and penetration into Vero cells was performed as previously described with modifications (Krawczyk et al., 2011). In brief, for the virus adsorption assay, prechilled (4 ℃ for 15 min) Vero cell were infected with HSV-2 (100 PFU/well) at 4 ℃ for 2 h in the absence or presence of serial concentrations (0, 0.02, 0.1, 0.2, 1, 10, or 100 μg/mL) of SHAP-1 or SHAP-2 to allow the virus binding to cells and prevented the virus from penetrating into cells. Unbound virus-polysaccharides incubation was removed and the cells were covered with agar overlay medium and incubated at 37 ℃ until plaques formed. For the virus penetration assay, prechilled (4 ℃ for 15 min), Vero cells were infected with HSV-2 (100 PFU/well) at 4 ℃ for 1 h to allow virus adsorption, then the unbound virus incubation was removed and serial dilutions of polysaccharides (0, 0.1, 1, 10, 100, 1000 μg/mL of SHAP-1 or SHAP-2) were added. The inoculated Vero cells were then incubated at 37 ℃ for 2 h to maximize penetration of the virus. Inhibitory efficacy was determined after 72 h as described above for the standard antiviral activity assay.

2.14. Statistical analysis

The data were expressed as mean ± standard error of the mean (SEM). Statistical analysis was performed using Graph Pad Prism 6. Significant differences were analyzed by two-way ANOVA test. P-values of less than 0.05 were considered as statistically significant. *, $p < 0.05$; **, $p < 0.01$; ***, $p < 0.001$; ****, $p < 0.0001$.

3. Results and discussion

3.1. Separation, isolation, and homogeneity of polysaccharides

The crude polysaccharide from *S. henslowianum* (SHCP) was obtained by hot water extraction, 80% EtOH precipitation, and dialysis. The yield was 5.1% based on the dried materials. From SHCP, two major fractions (SHN and SHA2) were obtained by ion-exchange chromatography on a DEAE 650 M column through a gradient elution by NaCl solution. Furthermore, the 1.0 M NaCl eluted fraction SHA2 was separated by the combination of ion-exchange column chromatography on DEAE 650 M and gel filtration chromatography on Sepharose 6 B and Sephacryl S-500 HR. As a result, polysaccharides SHAP-1 (688 mg) and SHAP-2 (445 mg) were obtained (Fig. 1).

SHAP-1 and SHAP-2 were purified as colorless powders. They both appeared as single and symmetrically sharp peak on the HPGPC chromatogram (Fig. 2). This characteristic suggests their homogeneity on the basis of molecular weight distribution. The apparent molecular weights of SHAP-1 and SHAP-2 were estimated to be 6.55×10^5 and 5.89×10^5, respectively, which were calculated from a dextran standard curve.

3.2. Structural features of SHAP-1 and SHAP-2

The contents of total carbohydrate, uronic acid, protein, and sulfate of SHAP-1 and SHAP-2 were determined, and results are shown in Table 1. Neither SHAP-1 nor SHAP-2 contains uronic acid. This result is different from those in reported fucoidans isolated from *S. henslowianum* (15.6%) (Han et al., 2018) and other brown algae in the genus *Sugassum*, such as *S. thunbergii* (56.24%) (Fu et al., 2018) and *S.*

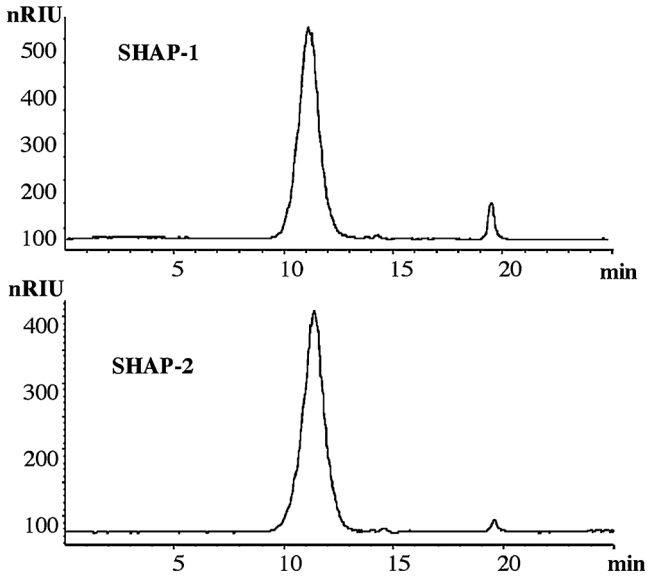

Fig. 2. High performance gel permission chromatogram (HPGPC) of purified polysaccharides named SHAP-1and SHAP-2. SHAP-1 and SHAP-2 were loaded on the PL aquagel-OH MIXED-H column (7.5 mm × 300 mm, 8 μm) in an Agilent 1260 Infinity II system equipped with ELSD and eluted with 0.1 M $NaNO_3$ at 0.6 mL/min with column temperature maintained at 35 °C.

Table 1
Chemical composition (%, w/w), and sugar composition (Area %) purified polysaccharides from *S. henslowianum*.

Polysaccharides	SHAP-1	SHAP-2
Chemical composition		
Total sugar content (%) [a]	61.1	45.8
Protein content (%)[b]	-*	–
Uronic acid content(%) [c]	–	–
Sulfate (%)[d]	31.92	31.89
Sugar composition		
Gal	23.7	25.1
Fuc	76.3	74.9

* Not be detected.
[a] Detected by phenol-H_2SO_4 method.
[b] Detected by Bio-Rad assay.
[c] Detected by m-hydroxyl biphenyl method.
[d] Detected by elemental analysis.

fusiforme (41.4%–61.31%) (Hu et al., 2016). In addition, element analysis showed that SHAP-1 and SHAP-2 contain relatively high amounts of sulfate groups (31.9%), suggesting that both SHAP-1 and SHAP-2 are highly sulfated polysaccharides. This result is higher than those in reported fucoidans isolated from this alga (21.4%) (Han et al., 2018) and *S. vulgare* (22.6%) (Dore, das C Faustino Alves, Will, Costa, & Sabry, 2013). The structural difference might be attributed to the fractionation process in addition to the different algal species.

Sugar composition analysis was performed by HPLC based on the pre-column PMP derivatization. As shown in Fig. 3, both SHAP-1 and SHAP-2 contain predominant amounts of fucose (Fuc) and small amounts of galactose (Gal) residues. This result suggests that SHAP-1 and SHAP-2 are highly sulfated heterogalactofucans, considering the high sulfate content. The compositional monosaccharides of SHAP-1 and SHAP-2 are in a Fuc*p*/Gal*p* ratio of 3 (Table 1). Compared with reported data in the genus *Sugassum*, the Fuc*p*/Gal*p* ratio is in accordance with fucoidans extracted from *S. gurjanovae* (3.11) (Cho et al., 2014; Prokofjeva et al., 2013; Usoltseva et al., 2018), higher than fucoidans derived from *S. duplicatum* (1.0) (Usoltseva et al., 2016, 2018, 2019) but lower than those in galactofucans from *S. cichorioides* (13.84)

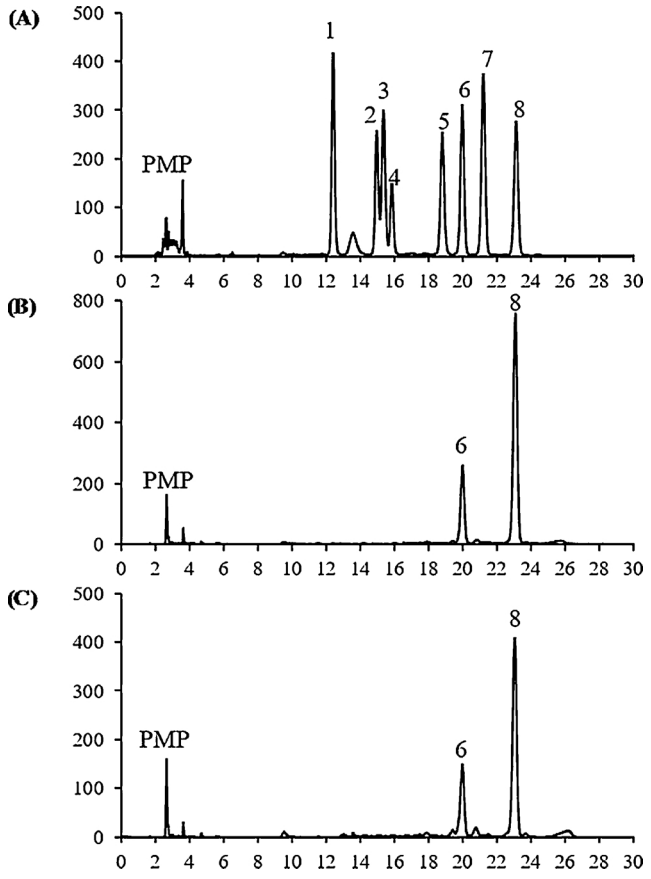

Fig. 3. The HPLC profiles of completely hydrolyzed and PMP derivatives of standards (A), SHAP-1 (B), SHAP-2 (C). 1-Man: mannose; 2-Rha: rhamnose; 3-GlcA: glucuronic acid; 4-GalA: galacturonic acid; 5-Glc: Glucose; 6-Gal: galactose; 7-Ara: arabinose; 8-Fuc: fucose.

(Prokofjeva et al., 2013). These results indicate the diversity of fucoidan structures even when they were isolated from the same genus.

FT-IR is broadly used to partially reveal the presence of characteristic functional groups of polysaccharides. SHAP-1 and SHAP-2 were further analyzed by FT-IR spectroscopy, as shown in Fig. 4A and B. The characteristic absorption band at 3373 cm^{-1} was assigned to hydroxyl group stretching vibration. The absorption signal at around 1617 cm^{-1} was attributed to the bending vibrations of HOH (Chen et al., 2013). The typical absorption band at approximately 1264 cm^{-1} was attributed to the asymmetric O═S═O stretching vibration of ester sulfate (Dore et al., 2013; Han et al., 2018). The results verified that both SHAP-1 and SHAP-2 are sulfated fucoidans. In addition, the characteristic absorption band at 838 cm^{-1} in the fingerprint region indicated that the sulfate esters are mainly located on the axial C-4 of fucopyranosyl (Fuc*p*) units (Dore et al., 2013). After desulfation, the characteristic absorption bands at 800–1270 cm^{-1} corresponding to sulfate groups decreased remarkably. This result suggested that the desulfation was successfully performed, as deduced directly from the disappearance of the sulfate group vibration at 1256.15 cm^{-1}. In addition, the absence of the absorption signal around 1750 cm^{-1} indicates that both SHAP-1 and SHAP-2 do not contain uronic acids, which are consistent with chemical and sugar composition analyses.

Methylation analysis was carried out to confirm the linkage type of sugar residues and the position of sulfate groups in SHAP-1 and SHAP-2. The position of the sulfate groups was deduced by comparing the methylation results of native polysaccharides with their desulfated forms. Results are shown in Table 2. Fucose, as the major constructive component of glycosyl residue, predominantly exists in (1→2,3,4)-linked Fuc*p* residues in native SHAP-1 and SHAP-2. These glycosyl

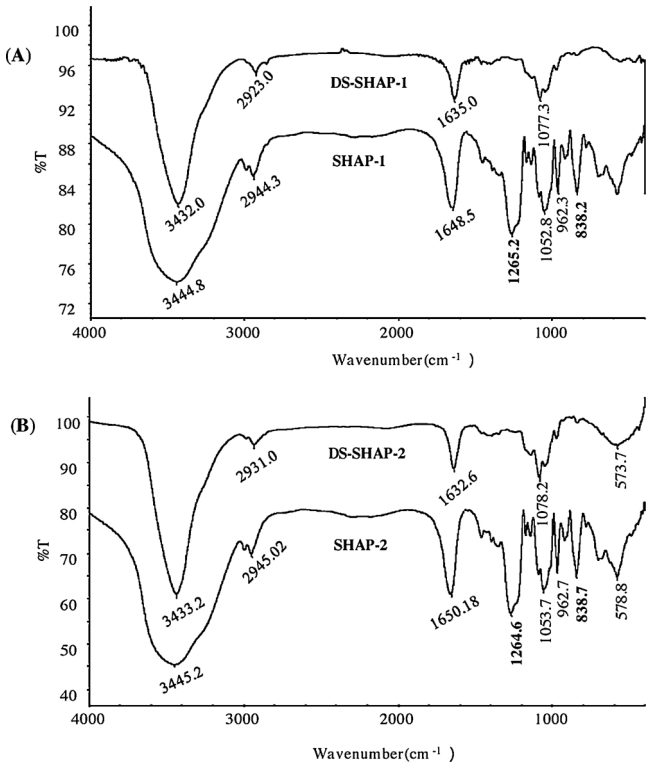

Fig. 4. FT-IR spectra of SHAP-1 and DS-SHAP-1 (A), SHAP-2 and DS-SHAP-2 (B).

Table 2
The linkages of polysaccharides determined by methylation and GC–MS.

Sugar	Type of linkage	SHAP-1	DS-SHAP-1	SHAP-2	DS-SHAP-2
Fuc					
	T*p*-	0.2	8.1	–	9.2
	1,4*p*-	0.4	3.1	–	3.7
	1,3*p*-	0.7	48.5	–	45.8
	1,3,4*p*-	2.6	11.7	0.3	14.4
	1,2,3*p*-	4.2	1.1	0.6	2.1
	1,2,4*p*-	–	2.7	–	2.3
	1,2,3,4*p*-	72.9	0.7	75.2	0.6
Gal					
	T*p*-	–	7.4	–	5.9
	1,2*p*-	–	6.8	–	6.1
	1,6*p*-	–	5.4	–	5.4
	1,2,6*p*-	–	3.1	–	3.3
	1,2,3,4,6*p*-	19.0	1.4	23.8	1.2

T: terminal; -: not detected.

residues in DS-SHAP-1 and DS-SHAP-2 decreased substantially to 0.7% and 0.6%, respectively. Meanwhile, (1→3)-linked Fuc*p* residues increased from trace amount up to more than 45%. These findings revealed that the backbone of both SHAP-1 and SHAP-2 consists of (1→3)-linked Fuc*p* residues, and the sulfate esters are mainly substituted at the C-2 and C-4 positions of (1→3)-linked Fuc*p* residues, which are consistent with the backbone of a fucoidan obtained from this alga by Cuong et al. Cuong et al. (2015). Furthermore, compared with native forms, terminally (*t*-), (1→4)-, (1→2,4)-, and (1→3,4)-linked Fuc*p* residues in desulfated forms increased obviously, suggesting that small amounts of sulfate esters are also located on the C-2,3,4 positions of *t*-linked Fuc*p*, the C-2,3 positions of (1→4)-linked, and the C-3 or C-2 position of (1→2,4)- or (1→3,4)-linked Fuc*p* residues. Moreover, the presence of relatively high amounts of (1→3,4)-linked Fuc*p* residues suggest that the backbone chain is mainly branched at the *O*-4 position of (1→3)-linked Fuc*p* residues. This characteristic is similar to those of

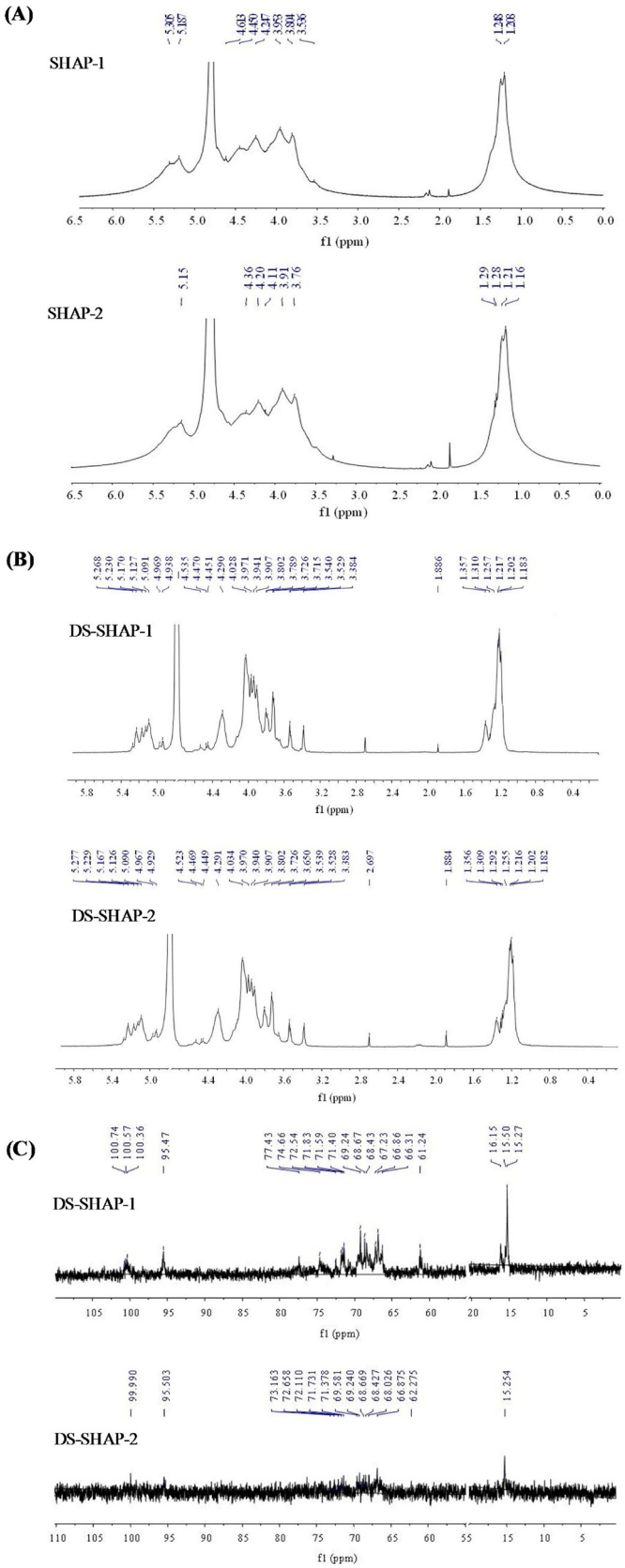

Fig. 5. ^{1}H-NMR (A) spectra of SHAP-1 and SHAP-2, and the ^{1}H- (B) and ^{13}C-NMR (C) spectra of desulfated forms (DS-SHAP-1, DS-SHAP-2) in D_2O at 25 ℃.

other fucoidans from brown algae (Bilan et al., 2018; Hentati et al., 2018). Different from other galactofucans in which Gal exists in terminal (1→3)- and (1→6)-linked Gal*p* residues (Bilan et al., 2018; Hentati et al., 2018), Gal in SHAP-1 and SHAP-2 appears in *t*-, (1→2)-, (1→6)-, (1→2,6)-linked Gal*p* residues in desufated forms. The absence of these residues in the native forms indicates that Gal residues are also sulfated. And sulfate groups occupy at the C-2,3,4,6, C-3,4,6, C-2,3,4, and/or C-3,4 positions of these residues. As described in literature (Bilan et al., 2018), these galactosyl residues as single or short side chain might be present in the periphery of the backbone, most possibly in *O*-4 of (1→3)-linked Fuc*p* residues. In conclusion, the above results suggest that SHAP-1 and SHAP-2 are of novel structural characteristic and of very high sulfate degree, which are different with previously reported sulfated polysaccharides isolated from *S. henslowianum* (Cuong et al., 2015; Han et al., 2018).

To further interpret the backbone structure of two fucoidans, 1D- and 2D-NMR experiments were performed. However, the 2D-NMR spectra could not be successfully recorded due to the low solubility (< 15 mg/mL) of either the original or desulfated samples. Because ^{1}H-NMR spectra (Fig. 5A) of SHAP-1 and SHAP-2 could not give enough proton information due to the high content of sulfate groups, the ^{1}H- and ^{13}C-NMR spectra of desulfated SHAP-1 (DS-SHAP-1) and SHAP-2 (DS-SHAP-2) are performed to assist the structural identification. Due to the weak signals on the ^{13}C-NMR spectra, the structural identification was mainly based on methylation and assisted by ^{1}H-NMR analyses, and comparison with reported data. In the ^{1}H-NMR spectra of both DS-SHAP-1 and DS-SHAP-2 (Fig. 5B), several important resonances appeared in the anomeric (δ 4.4–5.3 ppm) and high-field (δ 1.1–4.3 ppm) regions. The chemical shifts at δ 4.94–5.17 ppm were attributed to six anomeric protons of α-L-Fuc*p* residues, including *t*-, (1→3)-, (1→4)-, (1→2,3)-, (1→3,4)-, and (1→2,4)-linked α-L-Fuc*p* residues (Bilan et al., 2018). Compared with reported data (Bilan et al., 2018), the signals at δ 5.27 ppm were assigned to the anomeric proton H-1 of *t*-linked α-D-Gal*p*, and the signals at δ 4.45, 4.47, and 4.53 ppm were attributed to (1→2)-, (1→6)-, and (1→2,6)-linked β-D-Gal*p* residues. In the high field, intensive signals from δ 1.18 to 1.36 ppm originated from the Fuc*p* residues (Bandyopadhyay, Navid, Ghosh, Schnitzler, & Ray, 2011; Bilan et al., 2002). In addition, weak proton signals appeared at about δ 1.89 and 2.2 ppm, indicating the presence of small amounts of *O*-acetyl groups (Dore et al., 2013). Comparison with reported data described in the literature (Bilan et al., 2018; Ermakova et al., 2013; Pone et al., 2019) showed that the resonances in the anomeric region (δ 95–101 ppm) and δ 15–17 ppm in the ^{13}C-NMR spectra of DS-SHAP-1 (Fig. 5C) can be attributed to the C-1 and C-6 of the α-L-Fuc*p* residues, respectively. The signals around at δ 100.6 and 95.5 ppm were attributed to C-1 of (1→3)- and (1→3,4)-α-L-Fuc*p*, whereas those in the region δ 66–81 ppm were attributed to the C2–C5 carbon resonances of the Fuc*p* ring. The resonance of methyl groups (C-6 of α-L-Fuc*p*) appeared as a strong signal centered at δ 15.3 ppm. The signal at δ 61.2 ppm was attributed to C-6 of β-D-Gal*p* residues. In view of the weak signal in the ^{13}C-NMR spectra of DS-SHAP-2 (Fig. 5C), only three typical signals were identified, including methyl groups (C-6 of α-L-Fuc*p*) at δ 15.3 ppm, C-1 of (1→3)- and (1→3,4)-α-L-Fuc*p* at δ 100.0 and 95.5 ppm.

3.3. In vitro anti-HSV activity

The cytotoxic effect of the newly isolated polysaccharides on Vero cells was first investigated by the cell viability assay (Fig. 6A and A–S) and death cell ratio measured by flow cytometry (Fig. 6B). Although, it is about 10% and 20% of cytotoxicity at the concentration of 400 μg/mL of SHAP-2 and SHAP-1 respectively, the flow cytometry result showed that the cell viability of polysaccharides treated groups were the same like healthy cell control group. We also evaluated the cytotoxic effect by the trypan blue exclusion test. The results showed that no cytotoxic effect was observed even when the sample concentration was up to 5000 μg/mL, suggesting that these sulfated polysaccharides are safe for use. Then, we evaluated their inhibitory effects on HSV-1 and HSV-2 plaque formation. Results showed that both SHAP-1 and SHAP-2 inhibited HSV-1 (Fig. 6C) and HSV-2 (Fig. 6D) plaque formation in a dose-dependent manner, with about ~95% HSV-1 infection and about ~90% HSV-2 infection being inhibited at a sample concentration of 10 μg/mL. The IC_{50} values of SHAP-1 and SHAP-2 against HSV-1 were estimated to be 0.89 and 0.82 μg/mL by plaque reduction assay, respectively. Meanwhile, their IC_{50} values against HSV-2 were both as low as 0.48 μg/mL. These results suggested that both SHAP-1 and SHAP-2 have good anti-HSV activities, not only for HSV-2, but also for HSV-1.

According to the antiviral evaluation index SI, SHAP-1 and SHAP-2 had SI > 5000 for HSV-1 and SI > 10,000 for HSV-2, which was significantly superior to the antiviral effect of the current clinical drug Acyclovir (1000–3000) and the reference compound heparin (SI > 474 for HSV-2; SI > 833 for HSV-1) (Ponce et al., 2019). Meanwhile, SHAP-1 and SHAP-2 had higher anti-HSV-2 selectivity than anti-HSV-1, suggesting that SHAP-1 and SHAP-2 had great clinical value in HSV-2.

3.4. Anti-HSV mode of action

To elucidate how those polysaccharides work on HSV-2, we used time-of-addition experiments to determine the most sensitive phase during HSV-2 infection. Vero cell monolayers were infected with HSV-2, and SHAP-1 or SHAP-2 were added at a concentration of 0.1 or 1 μg/mL before, during, and after virus infection. As shown in Fig. 7, 1 μg/mL of SHAP-1 and SHAP-2 were observed to inhibit HSV-2 infection most efficiently when the samples were added during virus infection. While samples were added before (3 h b.i.) or after (0–10, 1–10, 3–10, and 6–10 h p.i.) the infection, no obvious antiviral activity was observed. These results suggest that SHAP-1 and SHAP-2 work in the early stage of infection, i.e., during virus adsorption to the host cell surface and/or virus penetration into host cells.

Adsorption and penetration assays were carried out to further characterize the mode of action of SHAP-1 and SHAP-2. We compared the inhibition efficacy of SHAP-1 and SHAP-2 when they were added before (adsorption) or after (penetration) HSV-2 virions interacted with Vero cells. As shown in Fig. 8A, SHAP-1 and SHAP-2 significantly interfered with virus adsorption to host cells in a dose-dependent manner, with about ~90% HSV-2 entry being inhibited at a concentration of 100 μg/mL. Meanwhile, penetration assay showed that SHAP-1 and SHAP-2 could respectively inhibit about ~40% and ~50% HSV-2 entry at a concentration of 1000 μg/mL (Fig. 8B). These results suggest that both SHAP-1 and SHAP-2 exert anit-HSV-2 infection mainly through the prevention of virus adsorption to host cell membranes.

Numerous sulfated polysaccharides are endowed with the capacity to inhibit herpetic infection by blocking the adsorption, penetration, and cell-to-cell spread of viruses (Ghosh et al., 2009). Among them, galactofucans show a high inhibitory activity against HSV-1 and HSV-2 with no cytotoxicity, whereas fucoidans containing uronic acid named uronofucoidans carry no antiviral activity (Ponce, Pujol, Damonte, Flores, & Stortz, 2003, 2019). These galactofucans have such structural characteristics with high sulfate groups and low level of uronic acid residues, suggesting that the uronic acid residues in fucoidan are not responsible for the antiviral activity, even blocking the antiviral effect. In support of this finding, SHAP-1 and SHAP-2 with high amounts of sulfate groups and without uronic acids showed strong anti-HSV activity, especially against HSV-2, in the present study. Additionally, the specific position of the sulfate groups is also important for the antiviral activity in addition to DS dependence (reviewed by Ghosh et al. (2009)). The high antiviral selectivity (SI > 5000 or SI > 10,000) of SHAP-1 and SHAP-2 in our study indicates that the C-2 and C-4 positions at the α-(1→3)-linked L-Fuc*p* backbone occupied by sulfate groups are responsible for the high anti-HSV activity. The relationship between structural characteristic and anti-HSV activity need to be further

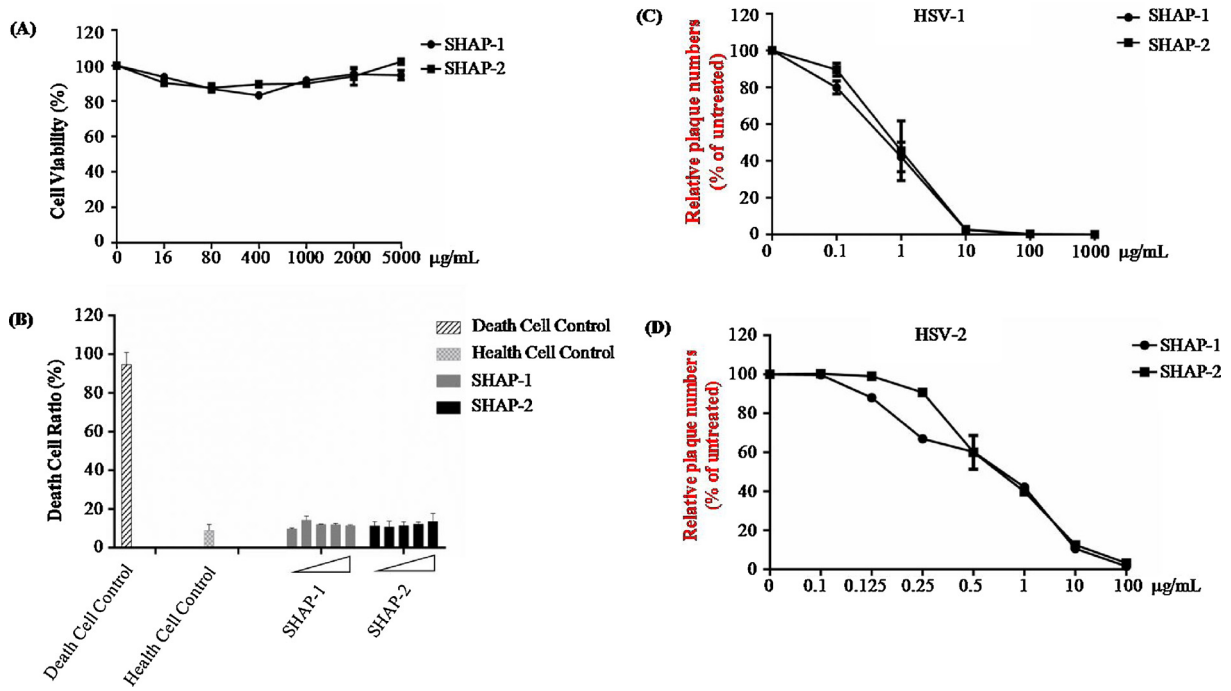

Fig. 6. Cytotoxicity and antiviral effects of SHAP-1 and SHAP-2. The cytotoxicity of SHAP-1 and SHAP-2 on Vero cells were evaluated by CCK-8 assay (A) and flow cytometry (B). Antiviral effects of SHAP-1 and SHAP-2 against HSV-1 (C) and HSV-2 (D) were performed as following: the confluent monolayers were infected with HSV-1 or HSV-2 (100 PFU/well) in the absence or presence of serial concentrations (0, 0.1, 1, 10,100, or 1000 µg/mL of SHAP-1 or SHAP-2 under HSV-1 infection and 0, 0.1, 0.125, 0.25, 0.5, 1, 10 or 100 µg/mL of SHAP-1 or SHAP-2 under HSV-2 infection) at 37 °C for 1 h. The cells were overlayed and further incubated at 37 °C for 72 h. The concentrations of compound required to reduce plaque number by 50% (IC_{50}). All data are expressed as mean ± SEM of triplicates.

investigated.

4. Conclusion

As described above, purified polysaccharides, SHAP-1 and SHAP-2, were isolated from the water extract of *S. henslowianum*. Elemental analysis revealed that SHAP-1 and SHAP-2 possess high contents of sulfate ester groups (31.92% and 31.89%, respectively). Structural analysis showed that both SHAP-1 and SHAP-2 contain fucosyl and galactosyl units at a ratio of 3:1. The backbone of these two sulfated galactofucoidans is composed of *α*-(1→3)-linked L-Fuc*p* residues, which are mainly branched at *O*-4 positions by side chains probably consisting of terminally linked *α*-L-Fuc*p* residues and *α*-D-Gal*p* residues, and (1→2)-, (1→6)-, and (1→2,6)-linked *β*-D-Gal*p* residues. The sulfate groups mainly occupied on the C-2 and C-4 positions of the main chain component residues. The backbone and the sulfated positions are consistent with the results reported by Cuong et al. (2015). In addition, a sulfated galactofucan from the brown alga *Hormophysa cuneiformis* features a similar backbone composed of *α*-L-Fucp residues. The branches composed of *t*-linked *α*-L-Fuc*p* (1→6)-linked *β*-D-Gal*p* residues were deduced to be attached at the *O*-4 position of backbone component residues (Bilan et al., 2018). This report also supports our findings, except for the linkage of component *β*-D-Gal*p* residues in side chains.

With the cytotoxicity assay, we found that the cytotoxicity of SHAP-1 and SHAP-2 is very weak. The CC_{50} values of SHAP-1 and SHAP-2 are both larger than 5000 µg/mL. Meanwhile, both polysaccharides exhibit significant anti-HSV activity to HSV-1F and HSV-2 333 strains. The IC_{50} values of SHAP-1 and SHAP-2 against HSV-1 were estimated to be 0.89 and 0.82 µg/mL by plaque reduction assay, respectively. Meanwhile, their IC_{50} values against HSV-2 were both as low as 0.48 µg/mL. Their SI values were larger than 5000 for HSV-1 and 10,000 for HSV-2. To the best of our knowledge, only few antiherpetic polysaccharides with so high antiherpetic SI value have been reported to date. Given their weak cytotoxicity and strong antiviral activities, SHAP-1 and SHAP-2 have potential clinical applications in individual or combination drug therapy.

Time-of-addition experiments were performed to understand the mechanism of action of these polysaccharides. SHAP-1 and SHAP-2

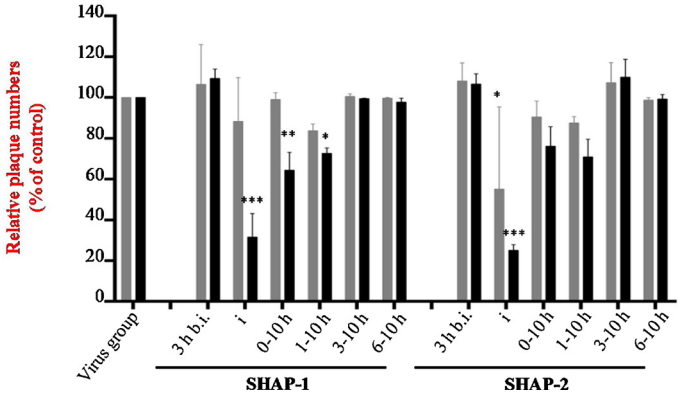

Fig. 7. Time-of-addition experiment of SHAP-1 and SHAP-2 against HSV-2. Vero cells were infected with HSV-2 (100 PFU/well). SHAP-1 and SHAP-2 (0.1 or 1.0 µg/mL) was added at various time intervals: 3 h before infection (3 h b.i.), during infection for 1 h (i), or after virus infection, at 0 h (0–10 h), 1 h (1–10 h), 3 h (3–10 h) and 6 h (6–10 h) post-infection (p.i.). No test compound was added to the control. At 10 h p.i., virus yields were determined by plaque assay. The plaque number of control was taken as 100%. Each value is the mean ± SEM from triplicate assays.

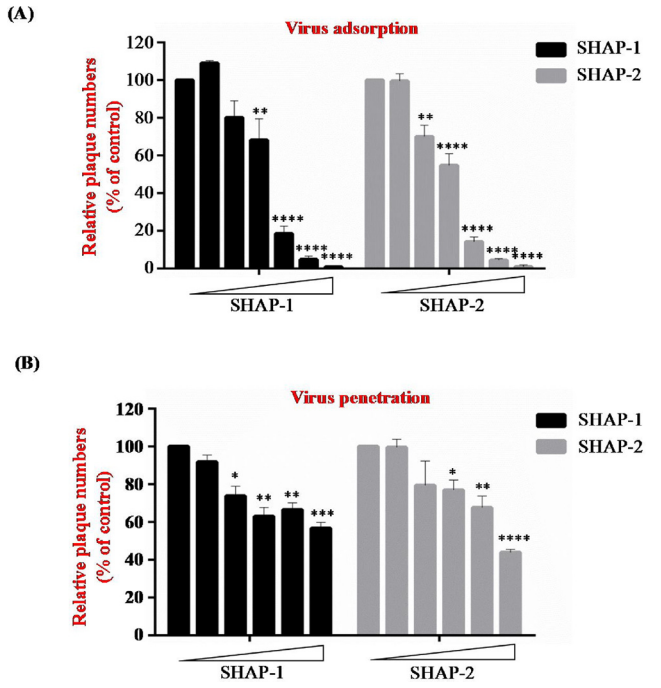

Fig. 8. Effect of SHAP-1 and SHAP-2 on HSV-2 adsorption and penetration. In adsorption assay (A), prechilled Vero monolayers were infected with HSV-2 (100 PFU/well) in the absence or presence of serial concentrations (0, 0.02, 0.1, 0.2, 1, 10 or 100 μg/mL) of SHAP-1 or SHAP-2 at 4 °C for 2 h. In penetration assay (B), prechilled cell monolayers were infected at 4°Cfor 1 h with HSV-2 in the absence of polysaccharides, and then shifted to 37 °Cfor 2 h in the absence or presence of polysaccharides (0, 0.1, 1, 10, 100 or 1000 μg/mL of SHAP-1 or SHAP-2) to penetrate the adsorbed virus. The incubation was removed and the cells wereincubated at 37 °C until plaques formed. The plaque number of no drug added was taken as 100%. Each value is the mean ± SEM from triplicate assays.

displayed their anti-HSV activities most efficiently when they were added during virus infection. This result agrees with the results of previous works, which indicated that polysaccharide has a potent anti-HSV activity at early stages of infection (Bouhlal et al., 2011; Zhu, Chiu, Ooi, Chan, & Ang, 2006). Furthermore, the results of adsorption and penetration assays indicated that SHAP-1 and SHAP-2 may prevent HSV-2 adsorption to host cell membranes.

Given its interesting characteristics and promising in vitro anti-HSV-2 properties, the fucoidans might be applied to prevent herpetic infections and represent a good candidate with a novel antiviral mode of action.

Acknowledgements

This work was supported by the National Natural Science Foundation of China [81803682] and partially sponsored by the project from Tianjin Key Laboratory on Technologies Enabling Development of Clinical Therapeutics and Diagnosis [CTD2018-03].

Appendix A. Supplementary data

Supplementary material related to this article can be found, in the online version, at doi:https://doi.org/10.1016/j.carbpol.2019.115487.

References

Ale, M. T., Maruyama, H., Tamauchi, H., Mikkelsen, J. D., & Meyer, A. S. (2011). Fucose-containing sulfated polysaccharides from brown seaweeds inhibit proliferation of melanoma cells and induce apoptosis by activation of caspase-3 in *vitro*. *Marine Drugs, 9*, 2605–2621.

Anastyuka, S. D., Shevchenko, N. M., Usoltseva, R. V., Silchenko, A. S., Zadorozhny, P. A., Dmitrenok, P. S., et al. (2017). Structural features and anticancer activity in *vitro* of fucoidan derivatives from brown alga *Saccharina cichorioides*. *Carbohydrate Polymers, 157*, 1503–1510.

Awasthi, S., Mahairas, G. G., Shaw, C. E., Huang, M. L., Koelle, D. M., Posavad, C., et al. (2015). A dual-modality herpes simplex virus 2 vaccine for preventing genital herpes by using glycoprotein C and D subunit antigens to induce potent antibody responses and adenovirus vectors containing capsid and tegument proteins as T cell immunogens. *Journal of Virology, 89*, 8497–8509.

Bandyopadhyay, S. S., Navid, M. H., Ghosh, T., Schnitzler, P., & Ray, B. (2011). Structural features and in *vitro* antiviral activities of sulfated polysaccharides from *Sphacelaria indica*. *Phytochemistry, 72*, 276–283.

Bilan, M. I., Grachev, A. A., Ustuzhanina, N. E., Shashkov, A. S., Nifantiev, N. E., & Usov, A. I. (2002). Structure of a fucoidan from the brown seaweed *Fucus evanescens* C. Ag. *Carbohydrate Research, 337*, 719–730.

Bilan, M. I., Ustyuzhanina, N. E., Shashkov, A. S., Thanh, T. T. T., Bui, M. L., Tran, T. T. V., et al. (2018). A sulfated galactofucan from the brown alga *Hormophysa cuneiformis* (Fucales, Sargassaceae). *Carbohydrate Research, 469*, 48–54.

Bouhlal, R., Haslin, C., Chermann, J. C., Colliec-Jouault, S., Sinquin, C., Simon, G., et al. (2011). Antiviral activities of sulfated polysaccharides isolated from *Sphaerococcus coronopifolius* (Rhodophytha, Gigartinales) and *Boergeseniella thuyoides* (Rhodophyta, Ceramiales). *Marine Drugs, 9*, 1187–1209.

Chatis, P. A., & Crumpacker, C. S. (1991). Analysis of the thymidine kinase gene from clinically isolated acyclovir-resistant herpes simplex viruses. *Virology, 2*, 793–797.

Chen, Y., Mao, W., Gao, Y., Teng, X., Zhu, W., Chen, Y., et al. (2013). Structural elucidation of an extracellular polysaccharide produced by the marine fungus *Aspergillus versicolor*. *Carbohydrate Polymers, 93*, 478–483.

Cho, M., Lee, D. J., Kim, J. K., & You, S. (2014). Molecular characterization and immunomodulatory activity of sulfated fucans from *Agarum cribrosum*. *Carbohydrate Polymers, 113*, 507–514.

Cho, Y., Cho, E. J., Lee, J., Yu, -H., Kim, S. J., Kim, Y. J., et al. (2016). Fucoidan-induced ID-1 suppression inhibits the in *vitro* and in *vivo* invasion of hepatocellular carcinoma cells. *Biomedecine & Pharmacotherapy, 83*, 607–616.

Ciucanu, I., & Kerek, F. (1984). A simple and rapid method for the permethylation of carbohydrates. *Carbohydrate Research, 131*, 209–217.

Cuong, H. D., Thuy, T. T., Huong, T. T., Ly, B. M., & Van, T. T. (2015). Structure and hypolipidaemic activity of fucoidan extracted from brown seaweed *Sargassum henslowianum*. *Natural Product Research, 29*, 411–415.

Dore, C. M., das C Faustino Alves, M. G., Will, L. S., Costa, T. G., Sabry, D. A., et al. (2013). A sulfated polysaccharide, fucans, isolated from brown algae *Sargassum vulgare* with anticoagulant, antithrombotic, antioxidant and anti-inflammatory effects. *Carbohydrate Polymers, 91*, 467–475.

Du, R. K., Wang, L. L., Xu, H., Wang, Z. Y., Zhang, T., Wang, M. L., et al. (2017). A novel glycoprotein D-specific monoclonal antibody neutralizes herpes simplex virus. *Antiviral Research, 147*, 131–141.

Dubois, M., Gilles, K. A., Hamilton, J. K., Rebers, P. A., & Smith, F. (1956). Colorimetric method for determination of sugars and related substances. *Analytical Chemistry, 28*, 350–356.

Ermakova, S., Men'shova, R., Vishchuk, O., Kim, S. M., Um, B.-H., Isakov, V., et al. (2013). Water-soluble polysaccharides from the brown alga *Eisenia bicyclis*: Structural characteristics and antitumor activity. *Algal Research, 2*, 51–58.

Finger-Jardim, F., Teixeira, L. O., de Oliveira, G. R., Barral, M. F., da Hora, V. P., Goncalves, C. V., et al. (2014). Herpes simplex virus: Prevalence in placental tissue and incidence in neonatal cord blood samples. *Journal of Medical Virology, 86*, 519–524.

Freeman, E. E., Weiss, H. A., Glynn, J. R., Cross, P. L., Whitworth, J. A., & Hayes, R. J. (2006). Herpes simplex virus 2 infection increases HIV acquisition in men and women: Systematic review and meta-analysis of longitudinal studies. *AIDS, 20*, 73–83.

Fu, X., Cao, C. L., Ren, B. B., Zhang, B., Huang, Q., & Li, C. (2018). Structural characterization and in vitro fermentation of a novel polysaccharide from *Sargassum thunbergii* and its impact on gut microbiota. *Carbohydrate Polymers, 183*, 230–239.

Ghosh, T., Chattopadhyay, K., Marschall, M., Karmakar, P., Mandal, P., & Ray, B. (2009). Focus on antivirally active sulfated polysaccharides: From structure-activity analysis to clinical evaluation. *Glycobiology, 19*, 2–15.

Gnann, J. W., Barton, N. H., & Whitley, R. J. (1983). Acyclovir: Mechanism of action, pharmacokinetics, safety and clinical applications. *Pharmacotherapy, 3*, 275–283.

Groves, M. J. (2016). Genital herpes: A review. *American Family Physician, 93*, 928–934.

GustavAsboe-Hansen, N. B. (1973). New method for quantitative determination of uranic acids. *Analytical Biochemistry, 54*, 484–489.

Han, M. H., Lee, D. S., Jeong, J. W., Hong, S. H., Choi, I. W., Cha, H. J., et al. (2017). Fucoidan induces ROS-dependent apoptosis in 5637 human bladder cancer cells by down regulating telomerase activity via inactivation of the PI3K/Akt signaling pathway. *Drug Development Research, 78*, 37–48.

Han, M. Y., Sun, P. C., Li, Y. Y., Wu, G., & Nie, J. W. (2018). Structural characterization of a polysaccharide from *Sargassum henslowianum* and its immunomodulatory effect on gastric cancer rat. *International Journal of Biological Macromolecules, 108*, 1120–1127.

Hentati, F., Delattre, C., Ursu, A. V., Desbrieres, J., Cerf, L. D., Gardarin, C., et al. (2018). Structural characterization and antioxidant activity of water-soluble polysaccharides from the tunisian brown seaweed *Cystoseira compressa*. *Carbohydrate Polymers, 198*, 589–600.

Honda, S., Akao, E., Suzuki, S., Okuda, M., Kakehi, K., & Nakamura, J. (1989). High performance liquid chromatorgraphy of reducing carbohydrates as strongly ultraviolet-absorbing and electrochemically sensitive 1-phenyl-3-methyl-5-pyrazolone derivatives. *Analytical Biochemistry, 180*, 351–357.

Hsu, H. Y., Lin, T. Y., Lu, M. K., Leng, P. J., Tsao, S. M., & Wu, Y. C. (2017). Fucoidan

induces Toll-like receptor 4-regulated reactive oxygen species and promotes endoplasmic reticulum stress-mediated apoptosis in lung cancer. *Scientific Reports, 7*, 44990.
Hu, P., Li, Z. X., Chen, M. C., Sun, Z. L., Ling, Y., Jiang, J., et al. (2016). Structural elucidation and protective role of a polysaccharide from *Sargassum fusiforme* on ameliorating learning and memory deficiencies in mice. *Carbohydrate Polymers, 139*, 150–158.
Islam, M. N., Ishita, I. J., Jin, S. E., Choi, R. J., Lee, C. M., Kim, Y. S., et al. (2013). Anti-inflammatory activity of edible brown alga *Saccharina japonica* and its constituents pheophorbide and pheophytin in LPS-stimulated RAW264.7 macrophage cells. *Food and Chemical Toxicology, 55*, 541–548.
Jaishankar, D., & Shukla, D. (2016). Genital Herpes: Insights into sexually transmitted infectious disease. *Microbial Cell Factories, 3*, 438–450.
Krawczyk, A., Krauss, J., Eis-Hübinger, A. M., Däumer, M. P., Schwarzenbacher, R., Dittmer, U., et al. (2011). Impact of valency of a glycoprotein B-specific monoclonal antibody on neutralization of herpes simplex virus. *Journal of Virology, 85*, 1793–1803.
Kwak, J. Y. (2014). Fucoidan as a marine anticancer agent in preclinical development. *Marine Drugs, 12*, 851–870.
Lee, J. B., Takeshita, A., Hayashi, K., & Hayashi, T. (2011). Structures and antiviral activities of polysaccharides from *Sargassum trichophyllum*. *Carbohydrate Polymers, 86*, 995–999.
Lim, S. J., Aida, W. M. W., Maskat, M. Y., Latip, J., Badri, K. H., Hassan, O., et al. (2016). Characterisation of fucoidan extracted from Malaysian *Sargassum binderi*. *Food Chemistry, 209*, 267–273.
Looker, K. J., Magaret, A. S., May, M. T., Turner, K. M., Vickerman, P., Gottlieb, S. L., et al. (2015). Global and regional estimates of prevalent and incident herpes simplex virus type 1 infections in 2012. *PloS One, 10*, e0140765.
Looker, K. J., Magaret, A. S., May, M. T., Turner, K. M. E., Vickerman, P., Newman, L. M., et al. (2017). First estimates of the global and regional incidence of neonatal herpes infection. *The Lancet Global Health, 5*, e300–e309.
Nagasawa, K., Inoue, Y., & Tokuyasu, T. (1979). An improved method for the preparation of chondroitin by solvolytic desulfation of chondroitin sulfates. *Journal of Biochemistry, 86*, 1323–1329.
Pomin, V. H., & Mourao, P. A. (2008). Structure, biology, evolution, and medical importance of sulfated fucans and galactans. *Glycobiology, 18*, 1016–1027.
Ponce, N. M. A., Pujol, C. A., Damonte, E. B., Flores, M. L., & Stortz, C. A. (2003). Fucoidans from the brown seaweed *Adenocystis utricularis*: Extraction methods, antiviral activity and structural studies. *Carbohydrate Research, 338*, 153–165.
Ponce, N. M. A., Flores, M. L., Pujol, C. A., Becerra, M. B., Navarro, D. A., Cordoba, O., et al. (2019). Fucoidans from the phaeophyta *Scytosiphon lomentaria*: Chemical analysis and antiviral activity of the galactofucan component. *Carbohydrate Research, 478*, 18–24.
Posavad, C. M., Koelle, D. M., Shaughnessy, M. F., & Corey, L. (1997). Severe genital herpes infections in HIV-infected individuals with impaired herpes simplex virus-specific CD8+ cytotoxic T lymphocyte responses. *Proceedings of the National Academy of Sciences of the United States of America, 94*, 10289–10294.
Prokofjeva, M. M., Imbs, T. I., Shevchenko, N. M., Spirin, P. V., Horn, S., Fehse, B., et al. (2013). Fucoidans as potential inhibitors of HIV-1. *Marine Drugs, 11*, 3000–3014.
Roizman, B., Knipe, D. M., & Whitley, R. J. (2007). Herpes simplex viruses. In B. N. Fields, D. M. Knipe, & P. M. Howley (Eds.). *Fields virology* (pp. 2501–2601). New York, NY: Lippincott, Williams & Wilkins.
Rui, X., Pan, H. F., Shao, S. L., & Xu, X. M. (2017). Anti-tumor and anti-angiogenic effects of fucoidan on prostate cancer: Possible JAK-STAT3 pathway. *BMC Complementary and Alternative Medicine, 17*, 378.
Sanjeewa, K. K. A., Fernando, I. P. S., Kim, E. A., Ahn, G., Jee, Y., & Jeon, Y. J. (2017). Anti-inflammatory activity of a sulfated polysaccharide isolated from an enzymatic digest of brown seaweed *Sargassum horneri* in RAW264.7 cells. *Nutrition Research and Practice, 11*, 3–10.
Sanjeewa, K. K. A., Kang, N., Ahn, G., Jee, Y., Kim, Y. T., & Jeon, Y. J. (2018). Bioactive potentials of sulfated polysaccharides isolated from brown seaweed *Sargassum spp* in related to human health applications: A review. *Food Hydrocolloids, 81*, 200–208.
Schneider, T., Ehrig, K., Liewert, I., & Alban, S. (2015). Interference with the CXCL12/CXCR4 axis as potential antitumor strategy: Superiority of a sulfated galactofucan from the brown alga *Saccharina latissima* and fucoidan over heparins. *Glycobiology, 25*, 812–824.
Shukla, D., & Spear, P. G. (2001). Herpes viruses and heparan sulfate: An intimate relationship in aid of viral entry. *Journal of Clinical Investigation, 108*, 503–510.
Sinha, S., Astani, A., Ghosh, T., Schnitzler, P., & Ray, B. (2010). Polysaccharides from *Sargassum tenerrimum*: Structural features, chemical modification and anti-viral activity. *Phytochemistry, 71*, 235–242.
Swetter, S. M., Hill, E. L., Kern, E. R., Koelle, D. M., Posavad, C. M., Lawrence, W., et al. (1998). Chronic vulvar ulceration in an immunocompetent woman due to acyclovir-resistant, thymidine kinase-deficient herpes simplex virus. *Journal of Infectious Diseases, 177*, 543–550.
Thuy, T. T. T., Ly, B. M., Van, T. T. T., Quang, N. V., Tu, H. C., Zheng, Y., et al. (2015). Anti-HIV activity of fucoidans from three brown seaweed species. *Carbohydrate Polymers, 22*, 122–128.
Usoltseva, R. V., Anastyuk, S. D., Shevchenko, N. M., Zvyagintseva, T. N., & Ermakova, S. P. (2016). The comparison of structure and anticancer activity in *vitro* of polysaccharides from brown algae *Alaria marginata* and *A. angusta*. *Carbohydrate Polymers, 153*, 258–265.
Usoltseva, R. V., Anastyuk, S. D., Ishina, I. A., Isakov, V. V., Zvyagintseva, T. N., Thinh, P. D., et al. (2018). Structural characteristics and anticancer activity in *vitro* of fucoidan from brown alga *Padina boryana*. *Carbohydrate Polymers, 184*, 260–268.
Usoltseva, R. V., Shevchenko, N. M., Malyarenko, O. S., Anastyuk, S. D., Kasprik, A. E., Zvyagintsev, N. V., et al. (2019). Fucoidans from brown algae *Laminaria longipes* and *Saccharina cichorioides*: Structural characteristics, anticancer and radio sensitizing activity in *vitro*. *Carbohydrate Polymers, 221*, 157–165.
Wu, M. J., Wu, Y., Qu, M., Li, W., & Yan, X. F. (2013). Evaluation of antioxidant activities of water-soluble polysaccharides from brown alga *Hizikia fusiformis*. *International Journal of Biological Macromolecules, 56*, 28–33.
Zhang, W., Okimura, T., Xu, L., Zhang, L., Oda, T., Kwak, M., et al. (2016). Ascophyllan functions as an adjuvant to promote anti-cancer effect by dendritic cell activation. *Oncotarget, 7*, 19284–19298.
Zhu, W., Ooi, V. E., Chan, P. K., & Ang, P. O., Jr. (2003). Isolation and characterization of a sulfated polysaccharide from the brown alga *Sargassum patens* and determination of its anti-herpes activity. *Biochemistry and Cell Biology, 81*, 25–33.
Zhu, W., Ooi, V. E., Chan, P. K., & Ang, P. O., Jr. (2004). Antiviral property and mode of action of a sulphated polysaccharide from *Sargassum patens* against herpes simplex virus type 2. *International Journal of Antimicrobial Agents, 24*, 279–283.
Zhu, W., Chiu, L. C. M., Ooi, V. E. C., Chan, P. K. S., & Ang, P. O., Jr. (2006). Antiviral property and mechanisms of a sulphated polysaccharide from the brown alga *Sargassum patens* against herpes implex virus type 1. *Phytomedicine, 13*, 695–701.